LEARN HADRON COLLIDER PHYSICS IN 3 DAYS

HEIDI SCHELLMAN

Dept. of Physics and Astronomy Northwestern University Evanston, IL USA 60208

A brief overview of experimental hadron collider physics for theoretical physics students, illustrated with recent results from the DØ and CDF experiments at the Tevatron.

1. Introduction and Acknowledgements

Because these lectures are meant to be educational rather than cutting edge, I have gone into more detail than usual. Such details are usually only available in doctoral dissertations. In particular I have relied on the DØ Dissertations of Levan Babukhadia 12 , Robert Snihur 5 , Juan Estrada 9 and Florencia Canelli 10 .

I would also like to thank the organizers and participants at TASI04. Their questions shaped the direction of these lectures and raised many other questions I'm still working on.

2. The characters in the story

These lectures describe physics done at hadron colliders, which have had four historical phases.

- (1) During the 1970's protons were collided with protons at a center of mass energy of around 60 GeV at the CERN ISR. Supersymmetry didn't really exist yet as a prediction and it was not discovered at the ISR.
- (2) During the 1980's the UA1 and UA2 experiments at CERN took data on proton-anti-proton collisions at $\sqrt{s} = 540$ GeV. The W and Z bosons were discovered by these experiments. They were shut down in order to run the LEP e^-e^+ collider during the 90's. They wiped out many popular models but failed to find Supersymmetry, despite theoretical expectations that it would be there.

(3) During the late 80's through the mid 90's the CDF and DØ experiments ran at the Fermilab Tevatron, colliding protons and antiprotons at an energy of $\sqrt{s} = 1800$ GeV. The major discovery was the top quark. Precision measurements of the top and W masses were also performed. CDF installed a silicon vertex tracker which enhanced their top signal and started a program in B physics at hadron colliders.

CDF and DØ shut down for 5 years in the late 90's for a detector and accelerator upgrade. During this time, the CDF silicon tracker was replaced with an improved version and the DØ experiment added a solenoidal magnetic field and a silicon tracker and now has similar capabilities to CDF.

The accelerator upgrade led to an increased center of mass energy of $\sqrt{s}=1960~{\rm GeV}$ and peak luminosities of $10^{32}{\rm cm}^{-2}{\rm sec}^{-1}$. The cross section for inelastic proton anti-proton scatters at 1960 GeV is $60~{\rm mb}=6\times10^{26}{\rm cm}^{-2}{\rm sec}^{-1}$ which works out to 4.2 million interactions per second at the peak luminosity. The beams only cross 1.7M times/second so at peak luminosity, DØ and CDF are now seeing two or more inelastic scatters per beam crossing. DØ and CDF have already logged close to a factor of four more data than in the previous run and hope to multiply the current sample by another factor of 10 before the LHC turns on.

Supersymmetry has not been found at the Tevatron, despite expectations, and many more interesting models have been ruled out

(4) In the late 90's LEP was shut down so that CERN could finish construction of the Large Hadron Collider (LHC), scheduled to start running in 2007. This will be a proton-proton, not proton-anti-proton machine at $\sqrt{s} = 14,000$ GeV, 7 times the Tevatron energy. The LHC will have 4 detectors, two of which, CMS and Atlas, are general purpose detectors optimized for high p_{\perp} physics. The machine luminosity is expected to be $10^{33} - 10^{34} \text{cm}^{-2} \text{sec}^{-1}$ with close to 20 inelastic scatters per beam crossing at high luminosity.

Discovery of Supersymmetry is expected in the first months of LHC operation.

3

3. The Technical details

3.1. Luminosity

Luminosity measures the flux of particles capable of creating a reaction of interest. The number $N_{observed}$ of events observed in an experiment is

$$N_{observed} = \left[\sigma_{process} \times \epsilon_{detection} \times \int \mathcal{L}dt \right] + N_{background}$$
 (1)

where the observable $\sigma_{process}$ is the cross section for the process and should not depend on the experimental details, $\epsilon_{detection}$ is the probability that a signal event will be observed in a given detector, $\int \mathcal{L}dt$ is the Integrated Luminosity and $N_{background}$ are events from other processes that got counted incorrectly.

At colliders, the luminosity depends on both the beam intensities and the beam densities.

$$\mathcal{L} = f \frac{N_p N_{\overline{p}}}{4\pi \sigma_x \sigma_y} \tag{2}$$

where f is the frequency with which beam bunches cross (1.7 MHz at the Tevatron), N_p is the number of protons/bunch, $N_{\overline{p}}$ is the number of anti-protons/bunch and σ_x and σ_y are the gaussian sizes of the beam. See http://www-bd.fnal.gov/notifyservlet/www for the real-time numbers for the Tevatron. Typical beam sizes at hadron colliders are 20-100 μ ms and typical instantaneous luminosities are $5\times10^{31} {\rm cm}^{-2}\,{\rm sec}^{-1}$. For integrated luminosities, we normally use inverse pico-barns (1 pico-barn⁻¹ = $10^{36} {\rm cm}^{-2}$) as a unit. During a typical running week, which has around 200,000 seconds of beam in it, 7-10 pb⁻¹ of luminosity will be delivered to each of the Fermilab experiments. This means that if a particle has a production cross section of 100 fb, one a week will be produced (but probably not detected) at the Tevatron.

3.2. Overview of Collider detectors

Particle detectors at colliders have evolved to be pretty similar - the technologies used in each component differ but they all have the same basic layout. Starting at the interaction point, there is

• a tracking volume with almost no material and a high magnetic field. This is used to measure the trajectory of charged particles

- with high precision. It normally has an inner, high resolution section built of silicon to detect the decays of short lived particles and an outer tracker made of less expensive materials and optimized for momentum measurement.
- a 'calorimeter' made of very heavy material which absorbs and detects almost all strongly and electromagnetically interacting particles. It is normally divided in to a high Z electromagnetic part and a cheaper outside hadronic part.
- a muon detection system, which measures the momentum of any muons which make it through the calorimeter.

These different pieces are illustrated in the picture of the $D\emptyset$ detector (Figure 1). More detail on these components is given below.

3.3. Collider physics Basics

As theorists, you think of processes as one or two incoming fundamental particles interacting to form an interesting final state. In e^-e^+ physics this is a good approximation, but in hadron colliders it is an approximation and it turns out, a bad one. Most of my examples will be from proton anti-proton collisions at the Tevatron (since that's what I know) but I will include comments on the LHC which will collide protons with protons.

The problem is that your fundamental incoming partons, quarks and gluons, are delivered in protons and antiprotons. The hard collision of interest only occurs when partons with the right quantum numbers happen to have the right center of mass energy to make the desired final state. Most of the time, the hard collision involves partons with the wrong quantum numbers or the wrong energy and all you get, from your point of view, is junk. The longitudinal momentum distribution of the desired partons in the proton is described by Parton Distribution Functions or PDF's, which can be determined from other processes. But these are probabilities, not certainties. As a result, in a given proton-antiproton reaction you do not know the longitudinal momentum of the initial state although you can predict the distribution of such momenta for an ensemble of events. Figure 4 shows typical parton distribution functions for important partons such as u quarks and gluons.

The total cross section for a parton of type 1 and a parton of type 2 to scatter is the integral over the probability of finding those partons in the proton to begin (the PDF) with times the hard scattering matrix element. In the following, the hatted quantities refer to the hard parton scatter while

Figure 1. Side view of the DØ detector. The innermost area contains a silicon vertex detector surrounded radially by a scintillating fiber magnetic tracker. The intermediate region is the calorimeter, shown in more detail in the next figure, and the outermost system detects muons which have escaped from the calorimeter.

Figure 2. One quadrant of the DØ calorimeter illustrating the segmentation in pseudorapidity.

the unhatted quantities are for the proton/ antiproton system.

Since we don't know the longitudinal momentum for the initial state, we should use cylindrical coordinates. Unless the protons are polarized, the cross section should be symmetric in azimuth so the relevant variables are p_{\parallel} and p_{\perp} . The parton distributions can be written as

$$f_i(x;\mu) \tag{3}$$

where i is the parton flavor, $x = p_{parton}/p_{proton}$ is the fraction of the proton momentum carried by the parton and μ is an appropriate hard scattering scale for the interaction. In the absence of strong interactions between the quarks in the proton, the PDF's would be just a function of x but interactions introduce a log μ dependence.

$$\sigma(p+\overline{p}\to X) = \int \hat{\sigma}(1+2\to X;\mu) f_1(x_1;\mu) f_2(x_2;\mu) dx_1 dx_2 \qquad (4)$$

 $\hat{\sigma}$ is the quark scattering cross section, it depends on the scale μ but (in principle) the observable cross section σ does not. In practice, one guesses that μ is the hard scattering momentum scale Q, which is often assumed

Figure 3. What is really going on in a hadron collider, partons collide and a mess of target remnants and scattered particles ensues. In this event a u from the proton and $\overline{\mathbf{u}}$ from the anti-proton have produced a final state with many particles, mainly concentrated in two jets.

to be the mass (*c) of the final state object or the transverse momentum of the final state particles. For a detailed discussion you might wish to look at the CTEQ Handbook of Perturbative QCD 2 or other QCD texts.

The parton center of mass energy is:

$$\hat{s} = x_1 x_2 s = x_1 x_2 (2P_{beam})^2 \tag{5}$$

and the momentum of the parton center of mass is:

$$p_z(cm) = (x_1 - x_2)P_{beam} \tag{6}$$

$$p_{\perp}(cm) \simeq 0 \tag{7}$$

Figure 4. The parton distribution functions (times x) for u quarks (up), d quarks (down), Gluons (gluon) and u anti-quarks (upbar) at a typical collider momentum transfer of $Q=100{\rm GeV/c}$. This was generated with the online pdf plotter from the Durham database http://durpdg.dur.ac.uk/HEPDATA/PDF.

Figure 5 shows the first order hard scattering diagrams for proton antiproton scattering. Figure 6 shows the typical x and Q ranges for different experiments.

Figure 4 shows typical parton distribution functions at collider energies. If you look at the parton probabilities in Figure 4, you note that gluons are the most probable partons, except at the highest momentum fractions, and in fact, the cross section at very low p_{\perp} is dominated by gluon-gluon and quark-gluon scattering via the t channel.

Figure 5. First order diagrams for proton-anti-proton scattering. If one assumes that time runs bottom to top (the theorist's convention), the first column indicate exchange in the t channel, the second s channel exchange, the third the u channel and the 4th is a special QCD diagram.

3.4. The final state

Quarks and gluons do not appear as particles in the final state, instead they fragment into 'jets' of reasonably long-lived hadronic particles such as π^+ , π^- , π^0 , K^+ , K^- , K_L , K_S , η , η' , p, n etc. The π^0 , η decay quickly into photons. This jet of particles generally follows the path of the original quark or gluon but there are important problems in making that identification. These include:

• The final state particles are color neutral, while the quarks and

Figure 6. Kinematic coverage of various experiments.

gluons are not. This means that there is a color connection between the final state partons (and the remnants of the proton and antiproton in most cases).

Higher order diagrams cause jet splitting. Some models of jet production take only the leading order hard diagram and then do fragmentation of those jets using parton shower models while others attempt to include higher order hard scattering diagrams and then fragment them. The degree to which fragmentation is handled in the original matrix element or in the fragmentation model is a rapidly

evolving art form.

- Algorithms for finding the jets vary generally fast algorithms such as cones are hard to map onto theoretical observables while algorithms which are theoretically robust, such as the k_{perp} algorithm, are time consuming and prone to experimental biases. For a nice recent review see reference ⁷.
- The final state particles deposit energy in the detector in different ways finding and summing the energy can be quite difficult.

Figure 7 shows the production of a jet when a quark is knocked out of a proton (by a neutrino). In step a), the quark is knocked out but remains connected to the proton by its color charge. At some point the energy in the color field becomes so high that it is energetically favorable to produce a quark anti-quark pair b) which can neutralize some of the color field. In c) the color neutral objects have 'hadronized' to form real observable particles, in this case a neutron and two kaons.

3.5. Kinematics

You may, personally, be interested in Higgsino production but the total proton anti-proton scattering cross section is dominated by t channel exchange of a gluon. Because the backgrounds are dominated by t channel processes, which have factors of $1/t \propto \sin^{-2} \frac{\theta}{2}$ in the matrix element it was realized early on that the polar angle θ was a lousy variable for describing what one actually sees in most produced events, even though most interesting interactions involve s channel quark anti-quark annihilation.

Instead of the polar angle, the rapidity, y, is used.

$$y \equiv \frac{1}{2} \left(\frac{E + p_{\parallel}}{E - p_{\parallel}} \right) \tag{8}$$

$$E = \frac{1}{2}e^y \sqrt{m^2 + p_{\perp}^2} \tag{9}$$

The big deal about rapidity is that:

• Differences in rapidity Δy are Lorentz invariant for boosts along the z (or rapidity) axis. You can verify this for yourself. Because of this, Lorentz Invariant Phase Space can be written as

$$\frac{d^3p}{2E} = d\phi dy dp_{\perp}^2 = 2\pi dy dp_{\perp}^2 \tag{10}$$

Figure 7. Illustration of fragmentation when a quark is knocked out of a proton, for example in a neutrino interaction.

• and if you go to a frame where the rapidity of a final state object is 0, it has a polar angle of $\frac{\pi}{2}$ and small variations in y are

$$\delta y \approx \delta \theta + \mathcal{O}(\delta \theta)^3 \tag{11}$$

equivalent to small variations in the polar angle θ .

This means that one can define 'jet's of hadrons in $y-\phi$ space and achieve results similar to those one would get at 90° in $\theta-\phi$

space.

The rapidity of a particle of mass M has kinematic limits set by the total energy available for that particle.

$$E_{max} \ge \frac{1}{2} e^{y_{max}} M \tag{12}$$

$$y_{max} = \log \frac{\sqrt{s}}{M} \tag{13}$$

For example, at the Tevatron, Z^0 bosons will have rapidities of less than 3, while top quarks will be less than 2.3.

The actual rapidity distributions are determined by the product of parton distributions, which determines the longitudinal momentum distributions of interactions, but empirically, the rapidity distribution for soft processes is closely approximated by a constant distribution per unit rapidity within the kinematics limits.

For massless particles (which are a good approximation for the decay products of almost anything in a collider) , the rapidity y reduces to the pseudo-rapidity:

$$\eta = -\log(\tan\frac{\theta}{2})\tag{14}$$

Figure 1 shows a side view of the DØ detector at Fermilab. Figure 2 shows a quadrant of the calorimeter and illustrates the segmentation in pseudo-rapidity. Collider detectors are designed so that each detector element covers the same area in $\eta-\phi$ space. For example, at DØ the detector elements are 0.1×0.1 in size.

The utility of plotting things in $\eta - \phi - p_{perp}$ space is illustrated when one looks at real data. Figure 9 shows a normal space view of the objects detected in a very high energy parton scatter. The initial state partons carried more than half of the proton's momentum and scattered at around 90 degrees. Figure 10 shows a lego plot in $\eta - \phi - p_{\perp}$ coordinates of the energy flow in the final state. Figure 8 illustrates the different coordinate systems and their relationship.

4. Example 1: Jet production

Our first example will be the simple partonic scattering illustrated in Figure 5, where two initial state partons scatter into two or more final state partons. These results have been published in references ⁸, ¹³. Levan

Figure 8. Illustration of collider coordinates. The sphere at top left has lines drawn at rapidity intervals. The cylinder on the right is the same space after the transformation to rapidity space $\theta \to \eta$. The bottom left diagram shows the cylinder being unrolled to make an $\eta - \phi$ grid. Particles can then be plotted in $\eta \phi p_{perp}$ space.

Babukhadia's thesis 12 contains a full description of the methods used. The observed final state will consist of 2 or more jets. Because the major diagrams have matrix elements that go like 1/t or 1/s which act like $1/p_{\perp}^2$ and the parton distributions approximately go as $1/x(1-x)^n$, the jet spectrum falls off very rapidly with transverse momentum.

Figure 9. A very high energy event in the DØ detector. The boxes represent calorimeter towers, with blue boxes having higher energy than green ones, the purple line are charged tracks, the brown cylinders are momentum vectors for the jets. The momentum vector scale is set very low, the two largest jets extend far outside the picture.

4.1. Calorimetry

The jets of particles are a mix of hadrons and electrons, muons and photons from decays. The energy of these particles are measured in a calorimeter, a detector designed to destructively measure the total energy of particles which enter it.

4.1.1. Electromagnetic Calorimeter

Calorimeters normally consist of two sections, one optimized to have high Z and detect electromagnetic energy, and another optimized to be both dense and thick which lies behind the electromagnetic calorimeter and detects any

Figure 10. A lego plot of the same event. The calorimeter transverse momentum is plotted in $\eta-\phi$ coordinates. The two high energy jets are very visible. The strange patterns for $|\eta|>3$ are due to energy deposited by the beam particle remnants and a change in segmentation from 0.1 units to 0.2 in the far forward region.

hadronic particles which make it through the electromagnetic part. The typical scale for electromagnetic showers is the radiation length X_0 (1/e absorption length) which ranges between 14 meters in liquid hydrogen to 0.32 cm in Uranium. The best material for dense detectors is Platinum at 0.305 cm but it's a bit pricey. Thanks to the cold war, depleted Uranium is much cheaper.

Figure 11 attempts to explain photon detection. Electron detection is almost identical - a photon shower is just two electron showers superposed in some sense. The decays $\Upsilon(9460)$, $J/\Psi(3100)$ and Z^0 to two electrons provide a very accurate calibration for electromagnetic energy at the 0.1%

Figure 11. Illustration of a photon interacting destructively in some heavy material. The photon interacts with a nucleus, pair produces an electron positron pair. The typical length scale is X_0 . Those electrons then bremsstrahlung photons, again over a scale of X_0 , which then pair produce and the process continues. All of the energy ends up as ionization caused by the electrons passing through the material which can then be detected. A typical length for such a shower is $L=X_0\log E/E_c$ where $E_c\approx 700 {\rm MeV}/(Z+1)$ is the critical energy. See chapter 26 and 27 of the PDG 4 for a discussion.

level.

Figure 12 shows a simulation of 10 GeV electrons and photons hitting the CMS Electromagnetic Calorimeter which consists of Pb-W glass blocks.

Figure 12. Simulation of the interactions of 10 GeV photons and electrons in the CMS electromagnetic calorimeter.

4.1.2. Hadron Calorimetry

Unfortunately, a hadronic jet is not all electromagnetic and in addition to pions and kaons, contains neutrinos and muons from weak decays, which don't interact enough to deposit their full energy. Hadrons such as pions, kaons, protons and neutrons do deposit energy but over a much longer distance scale, the interaction length λ_I , which ranges from around 600 cm in liquid hydrogen to 10 cm in Uranium. Since the hadronic showers are generally much longer than electromagnetic showers, hadron calorimeters are generally put behind electromagnetic calorimeters and build of cheaper materials. Figure 13 shows a hadronic shower, it looks similar to an electron shower but the particles involved are more diverse and the length scales are much longer. Generally, hadronic calorimeters need to be 6-10 interaction lengths thick with the limiting factor being cost and mass. Figure 14, from

Figure 13. The shower induced by a charged pion. The length scale is much longer and the range of interactions at each stage is much more complex than in the electromagnetic case. In fact, if particles are moving slow enough they can undergo weak decays and muons and neutrinos can be produced which leave the calorimeter undetected. In this case, a sampling calorimeter is illustrated where liquid argon lies between uranium plates. The charged particles in the shower ionize the Argon and the electrons from the ionization are swept up by high voltage across the gap. Ionization in the uranium is not detected and a 'sampling' correction is applied for this loss.

the PDG ⁴ Chapter 27, shows measurements of the energy containment of hadron calorimeters vs energy and thickness. For hadronic calorimeters, which need to have lots of material, both for thickness and because other large parts of the detector are inside them, cheaper materials such as Fe or Cu are normally used with Liquid Argon or scintillator readout. Such calorimeters are 'sampling' calorimeters.

Figure 14. Energy containment in a hadronic calorimeter as a function of thickness and beam energy. The CCFR detector was an iron scintillator sandwich over 50 λ_I thick.

4.1.3. Sampling vs. non-sampling

Figure 13 also illustrates 'sampling'. Calorimeters can be made 100% active by using glasses such as Cs-I or Pb-W or liquid Xe. But 'sampling' calorimeters, in which an passive heavy material such as Uranium is interleaved with an active material, such as Argon or scintillating plastic, are much less expensive and usually used for large detectors. In these detectors a 'sampling' correction must be made for the fraction of energy lost in the passive material. The losses in the passive material cause statistical fluctuations in the amount of energy detected and substantially degrade the resolution of the detector. However, by appropriate choice of sampling fractions as a function of depth, the response of the calorimeter to photons (which interact early) and hadrons (which interact late) can be compensated, leading to smaller errors for jets with mixed electromagnetic and hadronic energies.

| $\frac{\sigma_E}{E}$ | detector type |
|----------------------------|--|
| $\frac{10-15\%}{\sqrt{E}}$ | Sampling Electromagnetic Calorimeter |
| $\frac{1-3\%}{\sqrt{E}}$ | Monolithic Electromagnetic Calorimeter |
| $\frac{35-60\%}{\sqrt{E}}$ | Sampling Hadronic Calorimeter |

4.1.4. Hadron Energy Calibration

Nature does not provide very many jet calibration lines. For example, the W and Z bosons decay to jets most of the time but the dijet cross section shows no appreciable enhancement around the mass peaks both due to poor resolution and a factor of $(\frac{\alpha}{\alpha_s})^2$ in electroweak cross sections relative to the QCD cross section. In future, when statistics are higher, the hadronic decays of W's in top decays should become a promising calibration point with much less background.

Jet scales are found either by a combination of Monte Carlo simulation and test beam measurements for individual particles or by in situ measurement of transverse momentum balance between photons and jets from the QCD/QED process $qG \to q\gamma$. After enormous effort, errors of the order of 3% on the energy scale can be achieved. ¹¹ is a 94 page article describing the procedure used by D0. 3% sounds good until you remember that the jet spectrum is falling very quickly as a function of the jet transverse momentum. This 3% error on the x (transverse momentum) axis quickly becomes a 30-50% error on the y (cross section) axis when the spectrum is falling fastest.

4.2. Result

Figures 15 and 16 summarizes the results from a measurement done at DØ in the late 90's. It is described in great detail in Levan Babukhadia's thesis 12 . The D0 result and a similar measurement from CDF have been published 8,13 . Figure 15 shows the p_{\perp} spectrum of jets for several rapidity bins. Figure 16 the p_{\perp} spectrum normalized to different theoretical predictions. The main source of variation in theoretical predictions is the input parton density functions, in particular, the gluon content at high x which is not well constrained by other experiments. The uncertainty on the measurement is completely dominated by the jet energy scale. What the plot does not show is that error is very highly correlated from point to point.

One can note that the MRST†g PDF set does match the data more closely and a full statistical analysis indicates that the better match is in

Figure 15. The transverse momentum spectrum for jets produced at center of mass energy 1800 GeV in the D0 detector.

fact significant. This has been interpreted as the presence of a larger gluon distribution at high x than had previously been believed. In particular, it indicates that a large fraction of the momentum of the proton can end up in a single gluon.

5. Simulations and neutrinos

Now that we've seen the QCD cross sections, we might want to look at how the others compare. Figure 17 shows the event rates for various processes in hadron-hadron collisions.

All other processes have much lower rates than the QCD rates discussed above and have to contend with huge backgrounds from simple QCD scatters in which the final state particles mimic something more interesting. For example, a W boson can decay to an electron and a neutrino, each with an energy of around 40 GeV in the W center of mass frame. This

Figure 16. Comparison of DØ jet data at 1800 GeV from the previous figure with two theoretical models, (\bullet) compares the data to the MRST \uparrow g PDF's while (\circ) compares to the more standard MRST set. The yellow bands indicate the systematic errors, which are completely dominated by the energy scale error.

leads to electrons and neutrinos with transverse momenta in the range 0-40 GeV, depending on the decay angle relative to the beam axis. The total cross section for this process at the Tevatron is around 2.6 nb once you take into account the branching fraction to electrons. The QCD cross section for producing 2 partons with transverse momenta of 25-40 GeV or above is roughly 2-10 μ barn or roughly a factor of a thousand higher. If your detector has a 0.1% chance of calling a QCD jet an electron, and messing up its transverse energy, you may be looking at a background as large as

Figure 17. Rates for various processes at Hadron colliders from reference []. The dashed vertical line shows the LHC energy. Note the curve labeled $E_T^{jet}>0.25$ TeV.

your signal. We have better ways of detecting W which will be described later, but one has to be very careful in detector design to measure rare processes in the presence of such large backgrounds.

5.1. QCD Backgrounds to rarer processes

There are several ways in which a normal quark can fragment in a way which looks like an electron, muon or neutrino in a detector.

- Jet fluctuations a jet of cm energy E > 40 resulting from a quark or gluon will have an average number $N_{chg} \simeq 7.7 \log_{10}(E/10 \text{ GeV}) + 1.3^{18}$ charged particles, mainly charged pions, and around $N_{neu} \simeq N_{chg}/2$ neutral pions in it. The neutral pions decay to two photons and hence look electromagnetic. Statistical fluctuations ^a can lead to N_{chg} being much smaller than the average, or the relative neutral and pion ratios changing radically in a small fraction of events. A small fraction of jets can either be intrinsically highly electromagnetic and electron like or have a single very energetic charged pion and little else.
- Decay in flight pions and kaons in the jet can decay in flight, mainly to muons.
- Dalitz decays and Photon interactions in the detector. A π^0 can decay to two photons and one can interact in the detector to form an electron-positron pair.
- Charm and B decay a small fraction of jets contain a b or c quark which carries most of the jet energy, the heavy quark can decay semileptonically, producing a muon or electron which carries a large fraction of the jet energy.
- Charge exchange reactions. A charged pion can turn into a neutral pion through a quasi-elastic charge exchange interaction in the calorimeter. This will look identical to an electron, with a charged particle pointing at an electromagnetic shower.

None of these are common - but when one has QCD rates that are thousands of times higher than the signal you are interested in, they become important.

5.2. Discussion of simulations

One way of studying and understanding the backgrounds is to simulate your process, the likely QCD backgrounds and the detector. I'm not going to talk about detector simulations and will concentrate on the methods used as inputs to the detector.

 $^{^{\}mathrm{a}}$ Which are not Poisson in N due to charge and flavor correlations, but even broader.

These simulations take the process you are interested in and produce real particles. These simulations differ in two ways from an analytical calculation of a cross section.

First, if you are going to do a detector simulation later on, your physics generator needs to generate real events with real 4-vectors, not just amplitudes or rates. And you get much faster convergence if all events have positive weights and preferably the same weight. Just generating events flat in phase space and then using your analytical calculation to assign a weight to each event is not going to work very well.

Second, nobody knows how to do a perturbative QCD calculation that produces real particles like pions - it would have to be very high order and still could not handle the non-perturbative hadronization phase.

Instead we rely on very useful codes such as PYTHIA ¹⁷ and HERWIG ¹⁹ which use parton showering or string models to convert partons into particles. These programs manage to simulate many of the interference effects you expect when you have colored particles radiating by using concepts such as angular ordering. Over the past 20 years, the parameters of the models have been tuned to match data from e^-e^+ , lepton-hadron and hadron-hadron scattering.

6. Neutrino detection at colliders

So far we've discussed the detection of electrons, photons and jets. Most interesting high p_{\perp} processes at colliders involve neutrinos or other non-interacting particles (such has hypothetical Lightest Supersymmetric Particle or LSSP). But even high energy neutrinos have a probability of only 10^{-10} of interacting in the typical hadron collider detector. While they cannot be detected, some of their parameters can be estimated by calculating the missing p_{\perp} in the event.

As noted earlier, we do not know the longitudinal momentum of the scattering quarks but we do have a pretty good idea what their transverse momenta are, close to zero. In principle, if you can measure the transverse momentum of every scattered particle $\overrightarrow{p_{\perp}}^{(i)}$, the transverse momentum of any non-interacting particle will be:

$$\vec{p}_{\perp} = -\sum_{i} \vec{p_{\perp}}^{(i)} \tag{15}$$

The magnitude of this variable is very frequently, and incorrectly, referred to as the missing Transverse Energy, E_{\perp} or MET. Which is reason-

able in the case of a neutrino but just plain wrong in the case of a 70 GeV LSSP or two neutrinos.

The missing transverse momentum estimate only works if the p_{\perp} and direction of all scattered particles except the missing particle are detected. This requires a 'Hermetic' detector which covers almost all of 4π solid angle with active components. Such coverage is very difficult and expensive to achieve. Detectors such as DØ and CDF have active calorimetry down to angles of order 3^o from the beam axis or rapidities out to ± 4 and are able to achieve p_{\perp} resolutions of order 5 GeV/c. However there is a potential for very large fluctuations in the missing momentum, for example if a jet fluctuates to be very electromagnetic in a calorimeter which responds differently to hadrons and electrons, exactly the kind of events which fake real electrons.

For events with one missing neutrino from a semi-leptonic decay, such as W boson production, the neutrino reconstruction is almost unambiguous. This is illustrated in Figure 18. However, di-boson production, leptonic top decays and almost any supersymmetric signal have multiple neutral particles in the final state and the missing momentum method can only yield the sum of the missing particles transverse momenta.

7. Example 2: The top quark at the Tevatron

7.1. Standard Model top production

Pairs of top quarks are produced either by quark-antiquark annihilation or gluon-gluon fusion. At the Tevatron, the cross section for this process is believed to be around 7 pb²². Single top can also be produced by electroweak diagrams with the exchange of a W but this process has not yet been observed.

The DØ and CDF collaborations have recorded an integrated luminosity of over 400 pb^{-1} each in run 1 and 2 combined. This means that the number of top-antitop pairs produced per experiment is:

$$N_{t\bar{t}} = \int \mathcal{L}dt \sigma_{t\bar{t}} = 7 \text{pb} * 400 \text{pb}^{-1} = 2800$$
 (16)

However, at the same time, the total QCD cross section for inelastic scatters is 60 mb.

$$N_{inel} = \int \mathcal{L}dt \sigma_{inel} = 60 \text{mb} * 400 \text{pb}^{-1} = 2.4 \times 10^{13}$$
 (17)

Figure 18. Illustration of W production and decay. The first 3 frames show the longitudinal view. The initial state consists of two quarks with different momenta, so the hard scatter is moving relative to the lab frame. The W is produced with a small recoil and then decays to a neutrino and an electron. The inset frame shows the view along the beam axis. The neutrino's $\overrightarrow{p}_{\perp}$ balances the transverse momenta of the recoil and the electron, but there is no information about the longitudinal component of the neutrino momentum.

So only one in 10^{10} interactions is a top event.

If there are not additional quark species and the CKM matrix is unitary, top is believed to decay .997 of the time to b+W with the W then decaying

to $e, \mu, \tau + \nu$ or to $\mathbf{u}, \mathbf{c} + \overline{\mathbf{d}}, \overline{\mathbf{s}}, \overline{\mathbf{b}}$. Figure 19 illustrates this process. Both kinds of W decay mode are problematic. In the case of leptonic decays, the neutrino leaves the detector without being detected while the hadronic modes look just like the 10^{10} QCD background events. Figure 20 shows the different W^+W^- decay signatures predicted for Standard Model top decays.

Figure 19. top anti-top production followed by the decays $t \to bW^+$, $\bar t \to \bar bW^-$ with one W decaying leptonically and the other hadronically.

7.2. Backgrounds

Typical energies for the leptons and jets produced in top decay are $\frac{m_t}{3}$ or 40-100 GeV and the total energy flowing transverse to the beam direction can be expected to be greater than 200 GeV. The major backgrounds to top production depend on the final state. For the all hadronic final state, the background is QCD going to 6 jets. For the semi-leptonic final states, the QCD/EW process W+jets mimics a top event, or one of the jets from a true QCD event can mimic an lepton and hence a W. The decays with two leptons have much lower backgrounds but are very rare and harder to

Figure 20. Fraction of $t\bar{t}$ events with different W^+W^- decay signatures. τ decays are lumped together. Note that decay modes involving e or μ^- are a small fraction of the total.

reconstruct because they have two neutrinos in the final state. For now I am going to concentrate on the semi-leptonic decays which have the signature $t \to b + \ell \nu$ and $\bar{t} \to \bar{b} + \bar{q}_1 q_2$ (and vice versa). The experimental signature is 4 jets, two of which contain bs while the other two should reconstruct to close to the W mass. The other W decays to a lepton ℓ and missing

transverse energy from the neutrino.

One of the major technologies that has made top detection much easier is tagging of b-jets. QCD backgrounds mainly consist of jets initiated by light quarks while top events should have 2 jets containing b quarks. Multilayer silicon vertex detector with resolutions in the 10-20 μ m range allow measurement of the decay length of long lived particles in jets, the presence of a long lived particle is a very strong signature for a b jet and hence a top quark. Figure 21 shows the region within 5 mm of a likely top interaction from CDF which shows two b tags. Figure 22 shows the transverse (xy) decay length distance L2 for a set of events from the CDF experiment which have passed all other top cuts. All of the backgrounds have lower L2 values than expected for top events.

So we have several experimental handles, the large transverse energy, the presence of a high p_{\perp} lepton, missing transverse momentum from the neutrino and the b-jets. A combination of all of these can now get a very clean top signal.

Figure 23 shows the number of jets found in CDF events with an identified leptonic W decay from and at least one tagged b jet. For total jet numbers of 3 and 4, the top signal becomes significant.

The CDF collaboration have recently submitted their new measurement of the top cross section in the dilepton channel at 1960 GeV to PRL 23 . It is

$$\sigma_{\rm t\bar{t}} = 7.0 \pm 2.4 (stat.) \pm 1.6 (syst.) \pm 0.4 (lum.)$$
 (18)

7.3. Top mass

The top mass is one of the most important parameters in the Standard model, because the top quark is heavy enough to have a significant influence on electroweak observables through virtual diagrams. These virtual diagrams lead to correlations between the masses of the W and t and the mass of the Higgs particle. New measurements of the top quark mass from D0's first run were recently published in Nature²⁵ and CDF have reported but not published results from their most recent running. The interesting part is that improved analysis techniques, better background rejection and calibration improvements have moved the central value to from 174 to $178 \pm 4.5 \text{ GeV}^{24}$. The effect of this changes is illustrated in Figure 24. The solid green line shows the combined W and top mass measurements from the Tevatron after addition of the more precise $D\emptyset$ measurement. The dashed line shows the previous values.

Figure 21. A top -antitop candidate from CDF viewed along the beam axis. Two separated vertices are found which indicate the presence of b-jets from top decay.

Figure 25 shows the effect of the change in the central value for the top mass on estimates of the Higgs mass.

7.4. Extraction of the top mass

The top mass can be measured with surprising precision - mainly because it is so high compared to the QCD scale of 1 GeV that strong interaction effects do not dominate, as they do in the determination of the other quark masses.

The basic method goes as follows. We have a top event with one semileptonic and 1 hadronic decay.

We know 5 momenta (those of the lepton, 2 jets from W decay and 2

Figure 22. Distribution of the transverse decay length for vertices in b jet candidates from CDF compared to backgrounds.

jets from b-decay) and the transverse portion of the neutrino momentum. We also assume that the lepton and neutrino are massless and can estimate the 'masses' of the jets. We can now start applying constraints.

First, the non-b jets come from a W and should have the appropriate mass.

Second, the lepton and neutrino should also reconstruct to the W mass. Here X_{\parallel} is the unknown longitudinal component of the neutrino momentum.

$$E_{\nu} = \sqrt{p_{\perp\nu}^2 + X_{\parallel}^2} \tag{19}$$

$$m_W^2 = (E_\ell + E_\nu)^2 - (\vec{p}_{\perp lepton} + \vec{p}_{\perp \nu})^2 - (p_{\parallel \ell} + X_{\parallel})^2$$
 (20)

This is a quadratic equation with two solutions for the neutrino momentum, and hence the W momentum.

We can then impose the remaining constraint, that the masses of the two tops must be equal and extract a top mass.

If detectors were perfect, that would be it but generally, top events have only 1 or zero tagged b jets and the charge of the b jet is not known so it

Figure 23. Distribution of the number of jets in addition to a W boson in events with at least one b quark identified by the CDF silicon vertex detector. Top events are expected to have 4 or more jets. A transverse energy cut of 200 GeV has been applied.

cannot be automatically associated with the W^+ or W^- . In general 12-14 combinations of objects must be considered and their consistency with the top anti-top hypothesis evaluated. In addition, b decays are weak decays and very likely to include neutrinos, which makes the energy determination for b jets different than that for ordinary jets.

Unfortunately, there are also a lot of background events out there as well which cannot be arbitrarily thrown out of the event sample.

The DØ collaboration very recently published 25 a determination of the top mass using likelihood methods. These methods have an advantage over the techniques used in previous analyses as configurations and events with smaller errors are given greater weight. The data sample used is from the previous run, where vertex tagging was not available to clean up the data sample or indicate which jets contained b quarks. Each combination of particles in each event had its log likelihood of being top or background calculated by comparison to a theoretical model as a function of the top mass. Figure 26 shows this distribution for a single event with a high likelihood for being top. This plot is the sum over all of the combinations.

Figure 24. LEPEWWG [24] plot of measurements of electroweak parameters vs. the masses of the top quark and W boson. The yellow bands represent different Standard Model Higgs masses. The solid green line shows the combined W and top mass measurements from the TeVatron after addition of the more precise DØ measurement. The dashed line shows the previous value.

is almost certainly background.

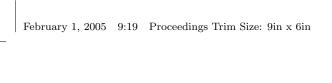
Figure 28 shows the log likelihood distribution for the ensemble of 71 events and the variation of likelihood as a function of the assumed mass near the peak. The optimal value after correction is $m_t = 180.1 \pm 5.3 \text{ GeV}/c^2$. This value is expected to improve greatly once the run II data are well understood as both DØ and CDF have larger statistics and much better b tagging. The dominant error remains the hadronic energy scale, which should also improve with better top signals as the W bosons in hadronic top decays are indeed the pure calibration line for hadronic energy scales we've needed for a decade.

Figure 25. Predictions [24] for the Standard Model Higgs mass. The dark blue dashed parabola shows the new best results with the improved top mass while the black parabola shows the results previous to 2004. The best estimate for the Higgs mass has risen substantially from 96 to 117 ${\rm GeV}/c^2$

8. Example 3: looking for the Higgs at Hadron colliders - or where is it anyways?

8.1. Standard Model Higgs production and decay

The Higgs is an excellent example of the difference between production and detection of rare signals. Because the Higgs couples to mass, Standard Model Higgs production generally involves t, W, Z either through loops or direct production. At the Tevatron, low mass Higgs bosons are produced via $GG \to top \ loop \to H(\text{Figure 29})$ and associated production (Figure





37

Figure 26. Negative Log Likelihood of the event kinematics for a single event with a very high likelihood of being a top.

Figure 27. Negative Log Likelihood of the event kinematics for a single event with a very small likelihood of being a top.

30 in which a quark and anti-quark produce a W^* which decays to WH. Figure 31 illustrates the relative production rates for these processes 27,26 at the Tevatron.

The Higgs also likes to decay into the highest mass particles possible.

Figure 28. Left: Combined log likelihood function for the 71 events in the sample. Right: the relative likelihoods for the various top masses considered.

Figure 29. Higgs production by gluon fusion.

Figure 32 shows the decay modes for low mass Higgs, below WW threshold, the Higgs has to decay to $b\bar{b}$ quarks. So for a Higgs just above the current limit of 114 GeV set by LEP, one would expect a Standard Model cross section for the process $q\bar{q}\to H\to b\bar{b}$ of 1 picobarn. During its best week in 2004, the Tevatron recorded over 20 inverse picobarns of data - or enough to produce 20 115 GeV Higgs going into $b\bar{b}$. Even if the Higgs mass were 200 GeV, the cross section for $GG\to toploop\to H\to WW$ is still over 0.1 picobarn so one would expect to see 2 or 3 in a good week. So why haven't you heard of the discovery or a new limit?

The reason is backgrounds, both due to particle misidentification and

Figure 30. Associated Higgs production.

real physics processes which have the same final state. In this case, it's likely that real physics is the problem. The total cross section for producing b or \bar{b} quarks at the Tevatron was recently measured by the CDF collaboration ³⁰ in the central (rapidity < 1) region. it is around 25 micro barns, or around 1/3,000 of the total proton anti-proton cross section. The cross section for producing $b\bar{b}$ is 1/2 that, but both CDF and DØ use twice the rapidity range for Higgs analysis as they did for this measurement, so the two factors cancel. This means, at typical luminosities, that 300-500 $b\bar{b}$ pairs are being produced per second, or 10,000,000 times the rate of $H \to b\bar{b}$ Most such b pairs are highly correlated and have a low invariant mass, but even 1 in a million is enough to swamp the Higgs signal.

8.2. Triggers and Detection

There are also instrumental problems in detecting the $b\bar{b}$ channel. Over 1 million proton-anti-proton interactions occur per second at the Tevatron, but only around 100 can be recorded due to limits on CPU and bandwidth.

Figure 31. Standard model Higgs cross sections at the Tevatron.

(Even so the Tevatron fills tapes faster than Fox News does). The rest of the events are eliminated by a multi-level trigger, which tries to distinguish interesting physics (in this case 2 b quarks) from backgrounds (light quark QCD).

CDF has a B physics trigger which relies on detection of the B decay length in the silicon tracker. The DØ B triggers rely more on the detection of muons in semi-leptonic B decay. Figure 33 illustrates the flow of data in the CDF trigger³¹. The Level 1 trigger makes a decision about the usefulness of an event (high energy, has a muon) in 5.5 microseconds. That crude decision takes the raw rate of around 1.5 Million events/second down to around 25,000/second ^b. A Level 2 trigger, which does fast tracking in the silicon detector and detects the separated vertex, reduces the data by a further factor of 100 to around 300/second which are then reduced to 100/second by running a full reconstruction program in Level 3. At each stage, real b's are lost and fake ones can slip through. One can estimate the probability of a simple $b\bar{b}$ event with a large invariant mass surviving by

^bThe 45 kHz is a peak number.

Figure 32. Standard model Higgs decay branching fractions from HDECAY.

considering the process $q\bar{q} \to Z \to b\bar{b}$ which has a cross section of around 15 nanobarns, about half way between the raw $b\bar{b}$ cross section and the Higgs.

Figure 34 shows a previous analysis of $Z \to b\bar{b}$ from the CDF experiment 30 . This was done with an earlier, less powerful, version of the new trigger and vertex detectors. The Z^0 is the slight enhancement above background on the falling edge of the background. The signal was $91 \pm 30 \pm 19$ events over a background of 250 observed in 110 inverse picobarns of data. This implies that the cross section for observing $Z \to b\bar{b}$ was around 1 picobarn, where the cross section for producing $Z \to b\bar{b}$ is around 1.5 nanobarns. CDF were only able to detect and identify 1/1,500 of the events with very large backgrounds. One should contrast this with the process $Z \to ee$ which has 1/5 the production cross section. 3,000 events with less than 1% background were observed in a data sample of similar size. For $Z \to ee$ the detection probability is of order 10% after triggering and holes in the detector are taken into account. Since those data were taken, CDF has

Figure 33. Diagram of the CDF trigger - three levels reduce the data rate from a potential $2.5~\mathrm{MHz}$ to $100~\mathrm{Hz}$.

added the separated vertex trigger, which should raise the $Z\to b\bar{b}$ signal substantially. But even with a good trigger, they won't see the 1 Higgs/week from $GG\to b\bar{b}$ the Standard Model suggests in our detectors.

8.3. The solution

There is a solution, look for rarer final states such as $Wb\bar{b}$ from associated production which have much lower backgrounds and higher trigger efficiencies. In particular, the presence of the W eliminates the need to trigger on a b quark. Figure 35 shows the data and background/signal sources for $Wb\bar{b}$ production at the DØ detector which was recently submitted to PRL 33 . The dominant backgrounds are real W+ continuum $b\bar{b}$ and top production. The limit set on Higgs production is around 10 times the expected Standard

Figure 34. CDF data on the decay $Z \to b\bar{b}$. The main drawing shows the background subtracted signal and the inset shows the raw data before background subtraction. The points are the data and the histogram is an estimate of the background shape from simulation.

Model cross section. The Tevatron Higgs Sensitivity study 26 done in 2003, indicated that integrated luminosities of 5,000-10,000 inverse picobarns will be necessary to see a Standard Model Higgs at the Tevatron.

9. Conclusions

I've discussed how particle detectors work at hadron colliders and the signatures for old and new physics. I've emphasized the problems in extracting rare signals from a very large background. I'll end with some advice for the aspiring theorist who wishes to have his/her ideas tested in the next 20 years.

Figure 35. Invariant mass of $H\to b\bar b$ candidates in the DØ detector. The points show the 5 data events while the histograms show various sources of backgrounds. The bump at the bottom is the signal expected from a Standard Model Higgs of mass 115 GeV.

- Rate alone cannot guarantee that a process you predict will be de-
- The key is special signatures final state electrons, muons, taus, heavy quarks, which are harder for QCD processes to mimic.
- To find truly rare processes, you probably need to use multiple special signatures.
- Get experimentalists interested in your physics so they don't throw it out at Level 1 in their trigger.

References

T. Sjöstrand, P. Edén, C. Friberg, L. Lönnblad, G. Miu, S. Mrenna and E. Norrbin, Computer Physics Commun. 135 (2001) 238. and hep-ph/0108264.

- 2. http://www.phys.psu.edu/≈cteq/handbook/v1.1/handbook.pdf
- R. Schwitters, "Jet Production in High Energy Hadron Collisions", Proceedings of the 11th Slac Summer Institute, P. McDonough editor, SLAC Report 267, 1984.
- Review of Particle Properties K. Hagiwara et al., Phys. Rev. D66, 010001 (2002)
- R. M. Snihur, "Subjet Multiplicity Of Quark And Gluon Jets Reconstructed With The K(T) Algorithm In P Anti-P Collisions,", Northwestern University Doctoral Dissertation, FERMILAB-THESIS-2000-25,
- D. Denegri, Standard Model physics at the LHC (pp collisions), 27 November 1990, Proceedings of the Large Hadron Collider Workshop, Aachen, 4-9 October 1990, Vol I,II,III, CERN 90-10.
- Jay Dittman, Talk given at the Jet/Met workshop at Fermilab, January 28, 2004. http://agenda.cern.ch/fullAgenda.php?ida=a04329.
- B. Abbott et al. [D0 Collaboration], "Inclusive jet production in p antip collisions," Phys. Rev. Lett. 86, 1707 (2001) [arXiv:hep-ex/0011036],
 V. M. Abazov et al. [D0 Collaboration], "Multiple jet production at low transverse energies in p anti-p collisions at s**(1/2) = 1.8-TeV," Phys. Rev. D 67, 052001 (2003) [arXiv:hep-ex/0207046]
- J. C. Estrada Vigil, "Maximal Use Of Kinematic Information For The Extraction Of The Mass Of The Top Quark In Single-Lepton T Anti-T Events At D0," Univ. of Rochester Doctoral Dissertation, FERMILAB-THESIS-2001-07,
- 10. M. F. Canelli, "Helicity of the W boson in single-lepton t anti-t events," FERMILAB-THESIS-2003-22
- 11. B. Abbott *et al.* [D0 Collaboration], "Determination of the absolute jet energy scale in the D0 calorimeters," Nucl. Instrum. Meth. A **424**, 352 (1999) [arXiv:hep-ex/9805009].
- L. R. Babukhadia, "Rapidity Dependence Of The Single Inclusive Jet Cross-Section In Proton - Anti-Proton Collisions At The Center-Of-Mass Energy Of 18-Tev With The D0 Detector,", University of Arizona Doctoral Dissertation, FERMILAB-THESIS-1999-03,
- 13. T. Affolder *et al.* [CDF Collaboration], Phys. Rev. D **64**, 032001 (2001) [Erratum-ibid. D **65**, 039903 (2002)] [arXiv:hep-ph/0102074].
- S. Frixione and B. R. Webber, "Matching NLO QCD computations and parton shower simulations," JHEP 0206, 029 (2002) [arXiv:hep-ph/0204244].S. Frixione and B. R. Webber, "The MC@NLO 2.3 event generator," arXiv:hep-ph/0402116.
- M. Kramer and D. E. Soper, "Next-to-leading order QCD calculations with parton showers. I: Collinear singularities," Phys. Rev. D 69, 054019 (2004) [arXiv:hep-ph/0306222].
- S. Mrenna and P. Richardson, "Matching matrix elements and parton showers with HERWIG and PYTHIA," JHEP 0405, 040 (2004) [arXiv:hep-ph/0312274].
- 17. T. Sjostrand, L. Lonnblad, S. Mrenna and P. Skands, "PYTHIA 6.3: Physics and manual," arXiv:hep-ph/0308153. T. Sjostrand, P. Eden, C. Friberg,

- L. Lonnblad, G. Miu, S. Mrenna and E. Norrbin, "High-energy-physics event generation with PYTHIA 6.1," Comput. Phys. Commun. **135**, 238 (2001) [arXiv:hep-ph/0010017].
- 18. T. Affolder *et al.* [CDF Collaboration], "Charged particle multiplicity in jets in p anti-p collisions at $s^{**}(1/2) = 1.8$ -TeV," Phys. Rev. Lett. **87**, 211804 (2001).
- G. Corcella et al., "HERWIG 6: An event generator for hadron emission reactions with interfering JHEP 0101, 010 (2001) [arXiv:hep-ph/0011363].
 G. Marchesini, B.R. Webber, G. Abbiendi, I.G. Knowles, M.H. Seymour and L. Stanco, Computer Phys. Commun. 67 (1992) 465.
- 20. Jason Nielsen, talk at the 2004 Lake Louise Winter Institute;
- 21. http://www-cdf.fnal.gov/physics/top/RunIIWjets/webpages/secvtx/public.html
- M. Cacciari, S. Frixione, M. L. Mangano, P. Nason and G. Ridolfi, "The t anti-t cross-section at 1.8-TeV and 1.96-TeV: A study of the systematics due to parton densities and scale dependence," JHEP **0404**, 068 (2004) [arXiv:hep-ph/0303085].
- 23. D. Acosta *et al.* [CDF Collaboration], "Measurement of the t anti-t production cross section in p anti-p collisions at $s^{**}(1/2) = 1.96$ -TeV using dilepton events," arXiv:hep-ex/0404036.
- 24. Lep Electroweak Working group and Tevatron Electroweak working group, http://lepewwg.web.cern.ch/LEPEWWG/, http://tevewwg.fnal.gov/i,
- V. M. Abazov et al. [D0 Collaboration], "A precision measurement of the mass of the top quark," Nature 429, 638 (2004).
- 26. L. Babukhadia *et al.* [CDF and D0 Working Group Members Collaboration], "Results of the Tevatron Higgs sensitivity study," FERMILAB-PUB-03-320-
- 27. T. Han and S. Willenbrock, "QCD correction to the p p \rightarrow W H and Z H total cross-sections," Phys. Lett. B **273**, 167 (1991).
- 28. A. Djouadi, J. Kalinowski and M. Spira, "HDECAY: A program for Higgs boson decays in the standard model and its supersymmetric extension," Comput. Phys. Commun. 108, 56 (1998) [arXiv:hep-ph/9704448].
- M. Spira, "Higgs boson production and decay at the Tevatron," arXiv:hep-ph/9810289.
- P. J. Bussey [CDF Collaboration], "Charm and beauty production at CDF," arXiv:hep-ex/0408020. M. Cacciari, S. Frixione, M. L. Mangano, P. Nason and G. Ridolfi, "QCD analysis of first b cross section data at 1.96-TeV," JHEP 0407, 033 (2004) [arXiv:hep-ph/0312132].
- 31. S. Baroiant *et al.* [CDF-II Collaboration], "The CDF-II tau physics program: Triggers, tau ID and preliminary results," arXiv:hep-ex/0312020.
- 32. T. Dorigo [CDF collaboration], "Observation of Z decays to b quark pairs at the Tevatron collider," arXiv:hep-ex/9806022.
- 33. V. M. Abazov et al. [D0 Collaboration], arXiv:hep-ex/0410062.